Hydraulic characteristics of stepped spillway dropshafts for urban deep tunnel drainage systems: the case study of Chengdu city

Lei Liao, Ruidong An, Jia Li, Wenmin Yi, Xiaofan Liu, Wenkang Meng and Lei Zhu

ABSTRACT

Cities in southwestern China experience urban drainage and overflow pollution after extreme rainfall events, which are major problems. In this study, a type of stepped spillway dropshaft suitable for drainage by deep tunnels in Chengdu was proposed and the hydraulic characteristics were investigated experimentally. The results showed that the nappe flow and strong turbulent deflected jet flow in the stepped spillway allowed the dropshaft to greatly dissipate energy. According to the distribution of the time-averaged pressure on the steps, the flow on the steps could be divided into a recirculating region, a wall-impinging region and a mixing region. The time-averaged pressure on the outside of the step was higher than that on the inside due to the centrifugal force effect of the water. The fluctuating pressure distribution of the step approximated the normal distribution. It was acceptable to calculate the minimum pressure with 3 times the root mean square (RMS). The vibration of the flow on the stepped spillway did not resonate with the step. When the outflow tunnel was under submerged outflow conditions, the aeration in the stepped spillway was exhausted through air holes and only a small amount of air entered the outflow tunnel, thereby avoiding an air explosion.

Key words | aeration, flow regime, fluctuating pressure, stepped dropshaft, time-averaged pressure

Lei Liao
Ruidong An (corresponding author)
Jia Li
Wenmin Yi
Xiaofan Liu
Wenkang Meng
Lei Zhu
State Key Laboratory of Hydraulics and Mountain River Engineering, College of Water Resource & Hydropower,
Sichuan University,
Chengdu 610065,
China
E-mail: *anruidong@scu.edu.cn*

INTRODUCTION

With the changes in global climate and the rapid development of urbanization, impervious urban areas have increased rapidly; however, the urban drainage standards have remained low, making urban drainage and overflow pollution control after extreme rainfall major problems in modern urban rainfall flood management (Board 2009; Fratini *et al.* 2012; Zhang *et al.* 2014).

Urban flood disasters have been particularly serious in China (Zhang *et al.* 2016; Zhou *et al.* 2017; Liang *et al.* 2019). Chengdu is the most important economic centre in Southwest China; however, frequent waterlogging disasters have caused very large economic losses and seriously threatened the safety of people's lives and property (Chen & Gao 2014). To solve this problem effectively, the urban drainage system required urgent updating. However, due to the constraints of the shallow underground space, difficulty of construction and high economic cost, it was not easy to transform the original underground drainage system (Liu *et al.* 2017). Urban deep tunnel drainage systems have become an important method of solving the problems of waterlogging and overflow pollution (Wang *et al.* 2016). For example, the deep tunnel drainage project in Lai Chi Kok in Hong Kong and the Chicago deep tunnel drainage project in the United States played an important role in local urban flood control and water quality improvement (Liu *et al.* 2017).

Urban deep tunnel drainage systems are mainly composed of an intercepting well and inlet pipe, dropshaft, main tunnel, surge shaft and drainage pump group (Hu *et al.* 2018). Dropshafts generally have a high hydraulic head and large discharge as well as aeration and air exhaust requirements (Granata 2016; Wu *et al.* 2018). However, certain hydraulic problems remain in the structure of the

doi: 10.2166/wst.2019.405

dropshafts that have been used in deep tunnel drainage systems. Although plunging and vortex dropshafts are simple in structure, due to the high flow velocity, the aeration of the water flowing into the deep tunnel is also large, and an air explosion is likely to occur at the exit of the tunnel under the condition of submerged outflow (Jain & Kennedy 1983; Jain 1988; Camino *et al.* 2014). The helicoidal-ramp dropshaft represented an improvement of the vortex dropshaft. The energy dissipation effect of the helicoidal-ramp dropshaft is better (Kennedy *et al.* 1988), although an adverse flow pattern of the water-wing on the external wall is easily formed under high-velocity flow conditions. The baffle dropshaft was skilfully equipped with a vertical wall structure for dry-wet separation and a special exhaust facility. By optimizing the diameter of the dropshaft, the space position of the baffle and the position of the vertical wall, negative pressure cannot occur in the dropshaft and the degree of aeration of the water entering the deep tunnel is very low; however, the structure has a higher requirement for baffle strength (Odgaard *et al.* 2013). The stepped spillway dropshaft was studied via turbulence numerical simulation. According to the numerical simulation results, the complex flow patterns in the stepped spillway were classified and the influence of the change in the central angle of the step on the flow pattern was analysed (Qi *et al.* 2018). However, the energy dissipation characteristics of the dropshaft and the aeration in the stepped spillway were not studied. The hydraulic characteristics of stepped spillway dropshafts at different step angles and end sill heights were studied (Shen *et al.* 2019). The results show that the stepped spillway dropshaft had a high energy dissipation rate. Although cavitation damage can be effectively avoided by aeration in the stepped spillway, the fluctuating pressure of the flow on the stepped spillway and the time-averaged water pressure change along the stepped spillway were not analysed.

In this paper, a type of stepped spillway dropshaft suitable for deep tunnel drainage in Chengdu is proposed. The flow regime, aeration, time-averaged pressure, energy dissipation characteristics and fluctuating pressure of the water flow in the stepped spillway dropshaft were analysed by physical model tests. The anti-cavitation performance of the dropshaft was analysed by the fluctuating pressure.

METHODS

Model description and measuring point layout

The model was designed according to gravity similarity, and its geometric scale was 1:14.4. The model was tested in the State Key Laboratory of Hydraulics and Mountain River Engineering, Sichuan University. A schematic structure of the model is shown in Figure 1. The stepped spillway dropshaft was mainly composed of the inlet channel (1), the dropshaft section (2) and the outlet channel (3). The length of the inlet and outlet channels was 173.6 cm. The cross section of the inlet and outlet channels was rectangular: 17.4 cm wide and 27.8 cm high. The dropshaft section consisted of the internal wall, the external wall and spiral steps. The external radius (R) of the dropshaft was 29.5 cm, and the internal radius (r) was 13.9 cm. The spiral steps consisted of horizontal and vertical steps. The height of each vertical step was 6.9 cm, the rotation angle of the horizontal step was 60 degrees, and the width of stepped spillway was 15.6 cm. The internal wall of the dropshaft innovatively formed the boundary of dry-wet separation. Air holes with a diameter of 5 cm were arranged on the internal wall of the dropshaft below each horizontal step level. Through these air holes, aeration and exhaust in the stepped spillway of the dropshaft can be realized. The height between the bottom plate of the shaft inlet channel and the bottom plate of the outlet channel was 430.5 cm. To observe the flow pattern and measure the hydraulic parameters, the model was made of transparent plexiglass.

Figure 2 shows the specific measuring positions of the pressure distribution on each step. Low pressure or negative pressure may occur near the vertical step because the flow on the stepped spillway occurred as a strong turbulent jet. Thus, P1 was chosen as a pressure test point on the vertical step. The water flow above the stepped spillway was different due to centrifugal force, resulting in different pressure behaviours on the outer side and the inner side of the horizontal step. Therefore, three pressure measuring points, P2, P3 and P4, were arranged outside the stepped spillway and two pressure measuring points, P5 and P6, were arranged inside the stepped spillway. To study the variation in pressure along the flow path, this study chose five steps to measure the pressure. Figure 1 shows the bottom elevation of the inlet channel, which was 0 cm in the direction of gravity, and the steps containing measurement points from top to bottom were S1, S2, S3, S4 and S5; the corresponding elevations were 62.5 cm, 104.2 cm, 187.5 cm, 270.8 cm and 312.5 cm, respectively.

Test conditions

In the study, a total of 3 hours of rainfall from 12:00 to 15:00 on March 1, 2017 were selected as the five-year rainfall data for Chengdu (Zhao *et al.* 2016). Through an analysis of the

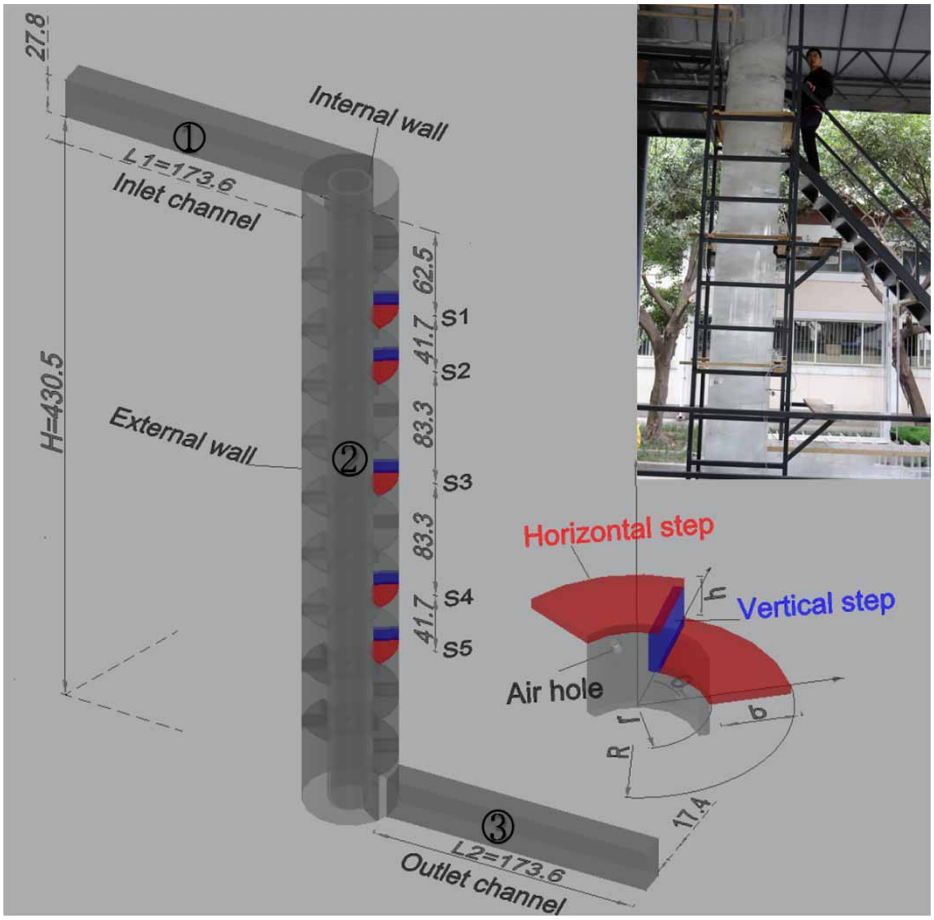

Figure 1 | Experimental setup: ① inlet channel; ② dropshaft section; ③ outlet channel; (unit: centimetre).

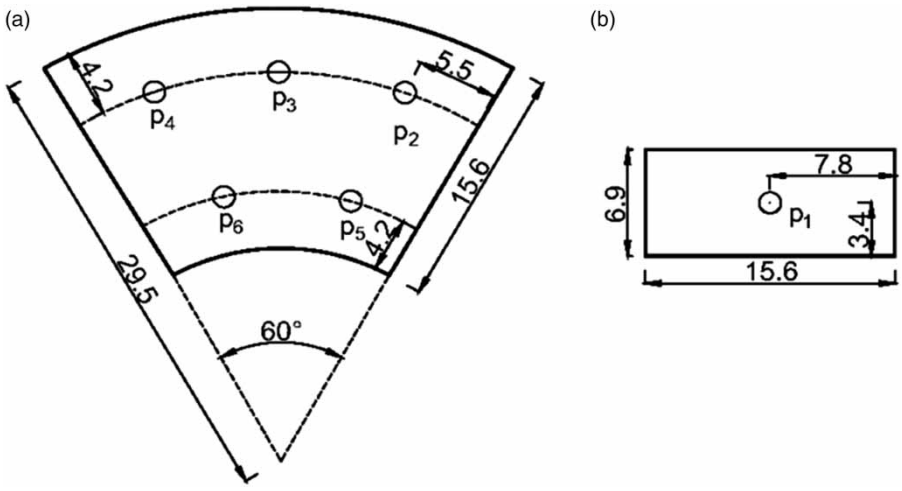

Figure 2 | Layout of the measuring points for the time-averaged hydrodynamic pressure and fluctuating pressure (unit: centimetre).

five-year rainfall process in Chengdu, the flow of the dropshaft was predicted and the simulated test conditions of the shaft were obtained (Table 1). The dimensionless discharge was calculated using Equation (1).

$$Q^* = Q/\sqrt{gb^5} \tag{1}$$

Table 1 | Test conditions of the stepped spillway dropshaft

Inflow discharge (m^3/s)	Q^*	Outflow status	Operation
5	0.21	Free outflow	Initial operation of the dropshaft
18	0.76	Free outflow	Initial rainfall runoff
18	0.76	Submerged outflow (20 m)	Initial rainfall runoff
30	1.26	Free outflow	Design of the discharge
30	1.26	Submerged outflow (20 m)	Design of the discharge
40	1.68	Free outflow	Peak flow
40	1.68	Submerged outflow (20 m)	Peak flow

Under submerged outflow conditions, the pressure head of outflow tunnel was 20 m.

where Q (m^3/s) is the discharge, g (m/s^2) is the acceleration of gravity, and b (m) is the stepped spillway width. The range of flow change in the experimental study was $Q = 5$–$40\ m^3/s$, which corresponded to $Q^* = 0.21$–1.68. The flow rate ($Q^* = 0.21$) was typical for the initial operation conditions of the dropshaft. Because the flow rate was low under these conditions, unfavourable hydraulic phenomena were not generated. Therefore, flow regime observation was only performed under these flow conditions, and pressure measurement analysis was not conducted. To ensure that the experimental results are consistent with actual engineering numerical equivalents, the values of the model test parameters were converted into prototype values.

Test methods

A high-speed camera was used to photograph and analyse the flow regime and aeration in the stepped spillway. An LGY-II intelligent velocity instrument produced by the Nanjing Hydraulic Research Institute was used to measure the flow velocity and then analyse the energy dissipation characteristics of the stepped spillway dropshaft under different flow conditions. The formula for calculating the energy dissipation rate of the stepped spillway dropshaft can be expressed as follows:

$$\eta = (E_1 - E_2)/E_1 \tag{2}$$

where η is the energy dissipation ratio, E_1 is the total energy of the section of the channel 15 m upstream of the dropshaft inlet, and E_2 was the total energy of the section of the channel 20 m downstream of the dropshaft outlet.

The equations for calculating the total energy of the inlet and outlet channels are expressed as follows:

$$E_1 = Z_1 + \frac{P_1}{\gamma} + \alpha_1 \frac{\tilde{v}_1}{2g} \tag{3}$$

$$E_2 = Z_2 + \frac{P_2}{\gamma} + \alpha_2 \frac{\tilde{v}_2}{2g} \tag{4}$$

where Z_1 and Z_2 are the elevation heads of the inflow and outflow, respectively; $P_1/\gamma = 0$ represents the pressure head when the entrance was an open channel; $P_2/\gamma = 0$ represents the pressure head when the outlet was under free outflow conditions; $P_2/\gamma = 20m$ represents the pressure head when the outlet was under submerged outflow conditions; $\tilde{v}_1$ and $\tilde{v}_2$ are the average velocities of the inflow and outflow sections, respectively; and $\alpha_1 = \alpha_2 = 1$.

A piezometric tube was used to measure the time-averaged hydrodynamic pressure on the vertical and horizontal steps. A high-precision digital pressure sensor, CY200, was used to measure the fluctuating pressure on the steps under different flow conditions. The experimental sampling frequency was 100 Hz, the sampling time was 20 seconds, and the sample size was 2,000. The root mean square (RMS) of fluctuating pressure represents the intensity of pressure fluctuation, and its calculation formula is as follows:

$$\sigma = \sqrt{\frac{1}{N}\sum_{n=1}^{N}(x_n - \bar{x})^2} \tag{5}$$

where x_n is the pressure at a given time and $\tilde{x}$ is the mean of the fluctuating pressure during the measurement period.

Generally, the coefficient of skewness (Cs) and coefficient of kurtosis (C_E) of the distribution are used to indicate the degree of deviation from the normal distribution. The calculation formulas for the skewness coefficient and kurtosis coefficient are as follows:

$$C_S = \frac{1}{N}\sum_{i=1}^{N}(x_i - \bar{x})^3/\sigma^3 \tag{6}$$

$$C_E = \frac{1}{N}\sum_{i=1}^{N}(x_i - \bar{x})^4/\sigma^4 \tag{7}$$

where x_i is the pressure at a given time, $\bar{x}$ is the mean of the fluctuating pressure during the measurement period, σ is the

RMS of fluctuating pressure and N is the total number of samples in a test series.

The instantaneous pressure in the stepped spillway was composed of the time-averaged pressure and fluctuating pressure. Even if the time-averaged pressure was higher than the critical pressure of cavitation, cavitation might occur due to the effect of the pulsating pressure. To study cavitation and cavitation erosion in the stepped spillway, the instantaneous number of cavitations in the stepped spillway was defined (Yu *et al.* 2010):

$$\sigma_{min} = \frac{p_{min}/\gamma + p_a/\gamma - p_v/\gamma}{v^2/2g} \tag{8}$$

where p_{min}/γ is the minimum instantaneous pressure of the measuring point, p_a/γ is the atmospheric pressure, p_v/γ is the saturated vapor pressure of water and $v^2/2g$ is the velocity head at the minimum instantaneous pressure.

RESULTS AND DISCUSSION

Flow regime and aeration

The flow regime on the stepped spillway is shown in Figure 3(a)–3(d), when the outlet channel was under free outflow conditions. Shen *et al.* found that supercritical flow in stepped spillways occurred when the rotation angle of the horizontal step was greater than or equal to 90 degrees (Shen *et al.* 2019). By analysing the flow patterns on the stepped spillway under different flow conditions, the flow patterns of this study were divided into the following three types.

(1) Nappe flow: when operating under low flow rate conditions ($Q^* = 0.21$), the water jet flowed onto the step by gravity, thus forming a relatively stable cavity below the water tongue; however, when the jet impacted the step, the water flow was broken. Since the flow rate and the flow velocity were low, there was only a small amount of milky white water flow on the surface of the jet, and the degree of aeration was low.
(2) Strong turbulent deflected jet: when the flow rate was high ($Q^* = 0.76$, $Q^* = 1.26$), the water flow in the stepped spillway was highly turbulent, and during the process of jet flow, the jet was deflected due to the curvature of the sidewall and the water depth on the outer side of the step was notably larger than that on the inner side. Recirculating vortices were formed below the concave corner of the step, and a considerable amount of milky white liquid was observed on the surface of the jet, and the degree of aeration was high. In this flow regime, the energy dissipation of the dropshaft occurred mainly through the strong turbulence of the jet, aeration, the impact of the jet on the steps, and the disruption of the water flow. In addition, when the discharge was 1.26, the water depth on the outer side of the stepped spillway was notably larger than that on the outer side of the stepped spillway when the discharge was 0.76.
(3) High flow rate: under a high flow rate ($Q^* = 1.68$), the flow on the outside of the step had a significant impact on the top of the step and potential safety hazards occurred.

The higher the flow rate, the higher the aeration degree on the stepped spillway; therefore, this study only analysed the exhaust problem of the dropshaft at a flow rate of 1.78. As shown in Figure 3(e), when the outlet was under submerged outflow conditions, the downstream tunnel pressure head was 20 m and hardly any aeration entered the outflow tunnel from the stepped spillway. Because of the pressure effect, the aeration in the stepped spillway was exhausted in the dropshaft through the air holes under the steps, and no air explosion would occur.

Time-averaged hydrodynamic pressure

An analysis of Figure 4 shows that the distribution of the time-averaged hydrodynamic pressure on each step basically remained the same when free outflow occurred under different working conditions. With the increase in flow rate (Q^*), the time-averaged hydrodynamic pressure on the step also increased. Based on the limited measuring points and the characteristics of the pressure distribution on each step, the flow on each step can be qualitatively divided into three regions.

Zone A was the recirculating region near the stepped concave angle, in which the water flow had distinct backflow characteristics and the pressure was low. Negative pressure (black circled area in Figure 4) occurred on the vertical step when Q^* was 0.76 and 1.26. When Q^* increased to 1.68, the pressure on the vertical step changed from negative pressure to low pressure, which was due to the increase of aeration in the stepped spillway when the flow rate increased.

Zone B was the wall-impinging region, which was near the maximum pressure on the horizontal stepped surface. The water flow in this area directly impacted the horizontal step; thus, the dynamic water pressure in this area was the maximum.

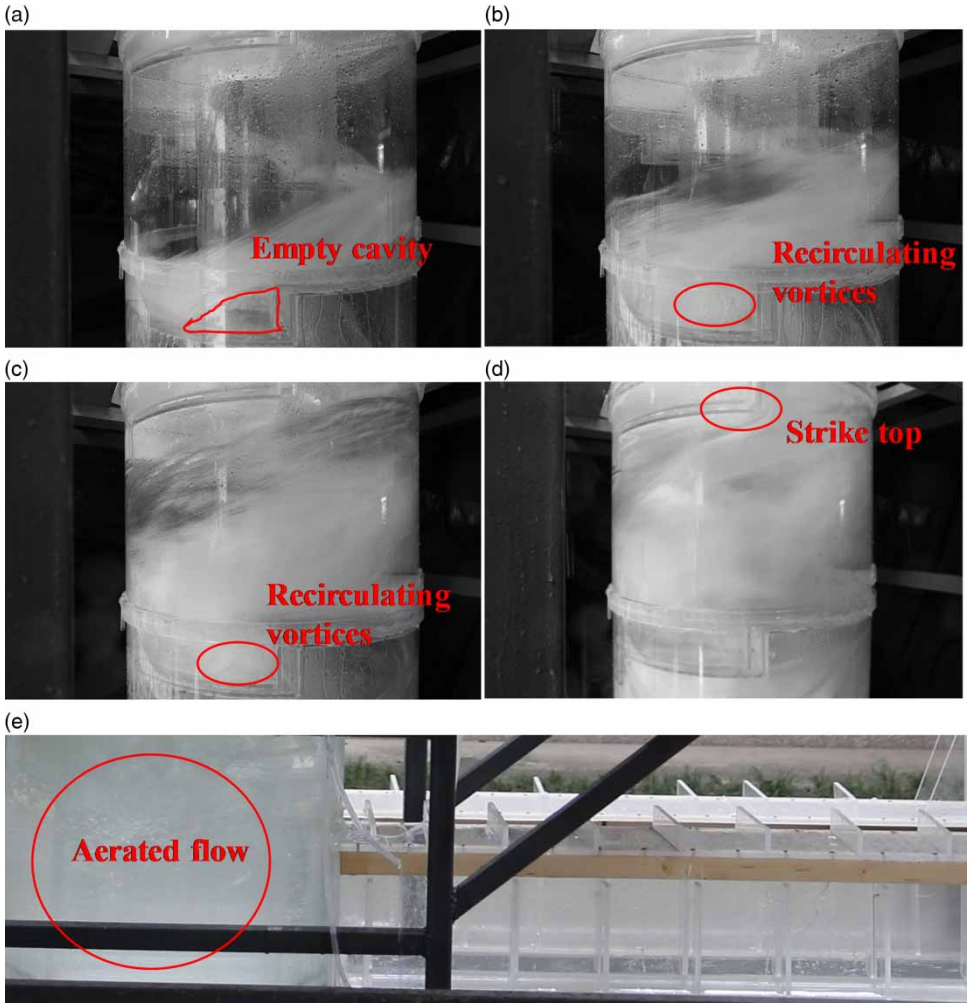

Figure 3 | Flow regime of the stepped spillway dropshaft.

Zone C was the mixed region, and the water flow was disrupted after impacting the horizontal step and became fully mixed at the end of the horizontal step.

When submerged outflow occurred under various working conditions, the distribution trend of the hydrodynamic pressure on the step of non-full flow was consistent with that under free flow conditions. Steps S4 and S5 were in the full flow state, and the distribution law of the hydrodynamic pressure was notably different from the pressure distribution law when free outflow occurred. When the flow above the step was in the full flow state, large pressure changes did not occur on the S4 and S5 steps, and with an increase in the submerged depth, the time-averaged hydrodynamic pressure on the S5 step was significantly higher than the time-averaged hydrodynamic pressure on the S4 step.

Figure 5 (S1, S2) shows that under the condition of free outflow at the same flow rate, the pressure P2 (P4) at the outside of the step was greater than that at the inside of the step, which was caused by the greater water depth at the outside of the step than that at the inside under the action of centrifugal force. Figure 5 (S4, S5) shows that under the condition of submerged outflow at the same flow rate, the pressure P2 (P4) at the point outside the step was almost equal to the pressure P5 (P6) at the point inside the step, which was due to the formation of full flow on the step when the flow was submerged and the water level inside and outside the step was the same.

Fluctuating pressure

The fluctuating pressure at each measuring point was dimensionless, and the relative fluctuating strength ($C_p = \sigma/h$) was defined, where h is the vertical step height. The analysis of Figure 6 shows that the distribution of the fluctuating

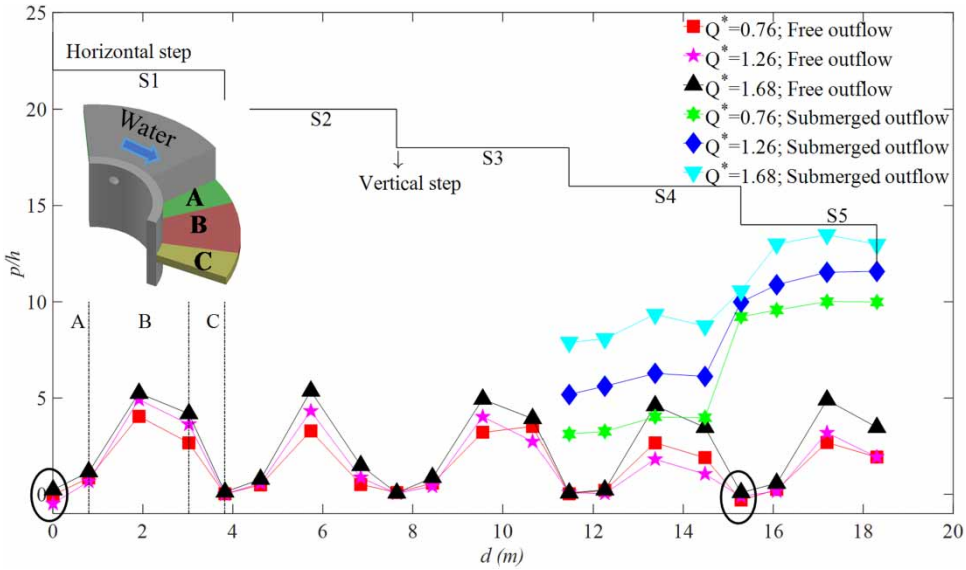

Figure 4 | Measurement results of the time-averaged hydrodynamic pressure on the outside of the horizontal step along the flow direction and the vertical step. The horizontal axis is the cumulative distance of the measuring points projected on the horizontal plane from the starting point of the step surface along the arc of the step surface in metres. The vertical axis is the ratio of the time-averaged hydrodynamic pressure to the vertical step height, and p/h is the dimensionless time-averaged hydrodynamic pressure.

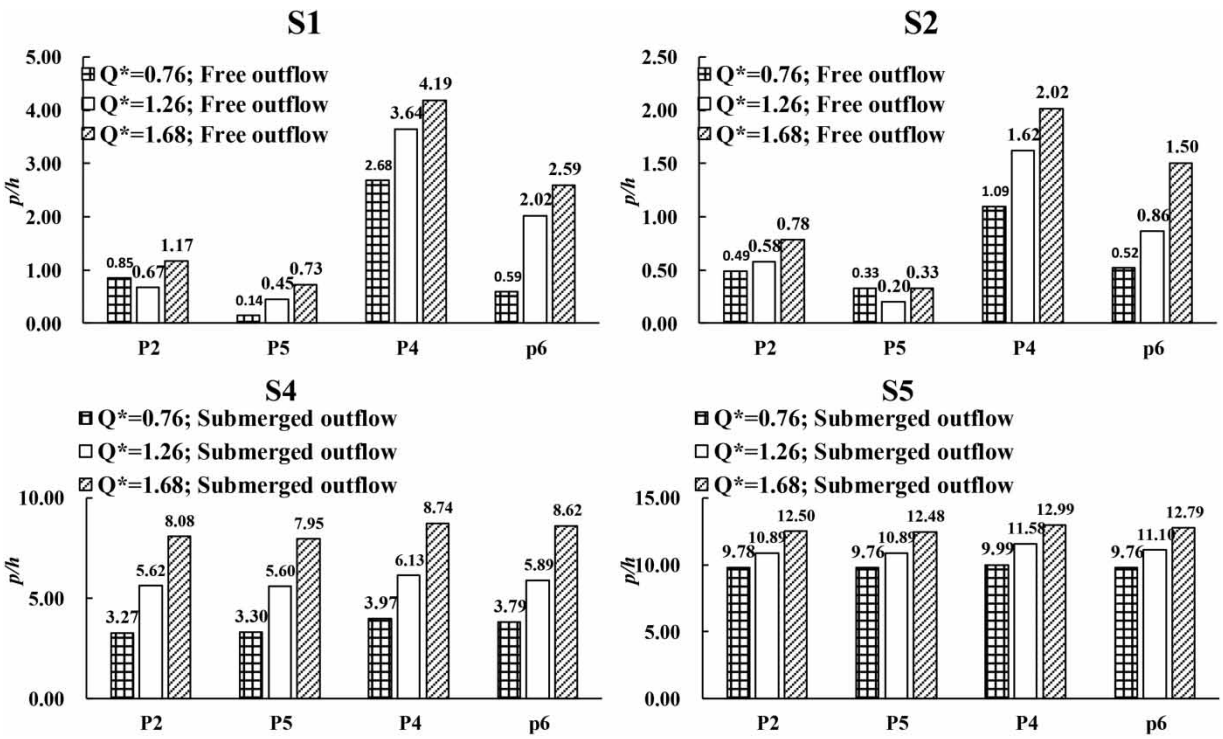

Figure 5 | Comparison of the time-averaged hydrodynamic pressure between the outer side and the inner side of the stepped spillway. The horizontal axis in the figure represents the position of the pressure tap on each step. The vertical axis is the ratio of the time-averaged hydrodynamic pressure to the vertical step height, and p/h is the dimensionless time-averaged hydrodynamic pressure.

strength on each step remained basically the same under free outflow conditions. Compared with the fluctuating strength, the maxima of each step basically occurred at the P4 measuring point, which was due to the direct impact of the water flow near the position on the horizontal step, resulting in a high fluctuating strength at the P4 point.

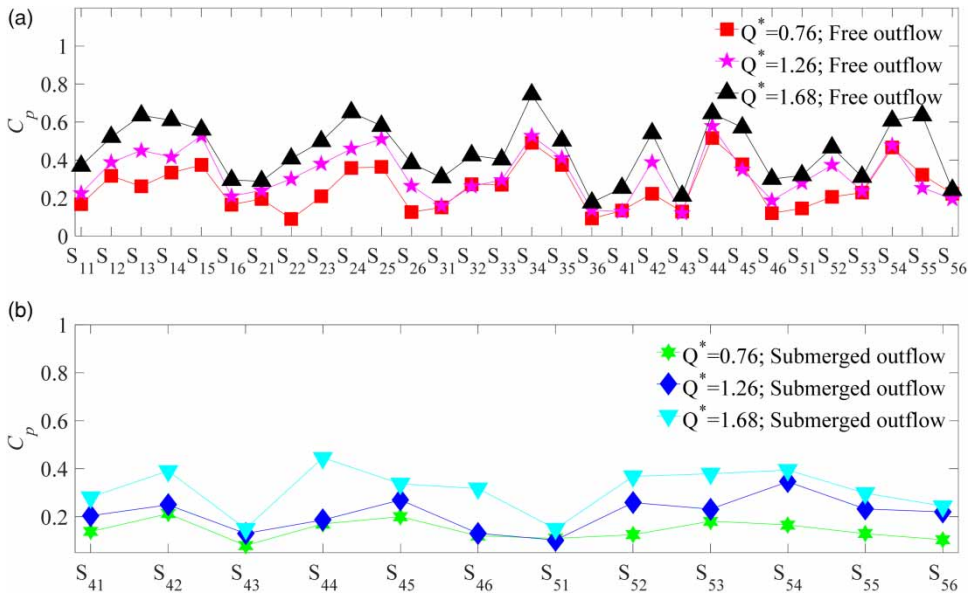

Figure 6 | Comparison of the fluctuating strength on the stepped spillway under various flow conditions. The horizontal axis in the figure represents the measurement position of the pulsating pressure on each step (S11 represents the position of the P1 measuring point on the step S1). The vertical axis in the figure indicates the comparison with the fluctuating strength.

Compared with the fluctuating strength, the minimal values of each step were observed in the concave and convex areas of the step, which was due to the recirculating and mixing areas of the flow. With the increase in the dimensionless flow rate, the fluctuating strength of each step also increased. Compared with submerged outflow, the change in the fluctuating strength on each step was more notable when free outflow occurred because when submerged outflow occurred, steps S4 and S5 were in the full flow state, and the turbulent deflection jet effect on the step was weakened, which resulted in little change compared with the fluctuating strength of the measured points in the full flow state of the step under submerged outflow conditions.

The maximum instantaneous pressure caused by the fluctuating pressure might cause scouring damage of the step surface, and the minimum instantaneous pressure might cause cavitation. If the magnitude of the main frequency and the dominant frequency of the fluctuating pressure were high and the range was wide, these conditions might cause strong vibration of the stepped spillway. The power spectrum of the fluctuating pressure indicated the energy distribution of the fluctuating flow in the frequency domain, which could be expressed by the power spectrum function. In this study, the main frequency of the fluctuating pressure was converted by the gravity similarity law, and the data of the fluctuating pressure were calculated by the fast Fourier transform. The main frequency was the frequency corresponding to the maximum energy value in the power spectrum diagram. Figure 7 shows that the energy of 95.08% of the fluctuating pressure is mainly concentrated within 15 Hz and the main frequency is 9.85 Hz. The natural frequencies of the first step of the sidewall and floor of the step are generally above 20 Hz (Chen 2014). The main frequency of the flow fluctuation in the stepped spillway was quite different from the natural frequency of stepped spillway, and almost no resonance of the stepped spillway occurred.

The probability density distribution function is an important characteristic of the amplitude of the pulsating pressure. The key question was whether the distribution was a normal distribution. The coefficient of skewness indicates the symmetry of the distribution. If $C_S = 0$, then the distribution is completely symmetrical. The coefficient of kurtosis indicates the degree of deviation between the peak height and that of the standard distribution. If $C_E = 3$, then the distribution is the standard positive distribution. Under the various flow conditions, the coefficients of skewness of each step were from -0.33 to 0.39 and the coefficients of kurtosis were from 0.13 to 2.01, which indicated that although the distribution of the fluctuating pressure in the stepped spillway was not completely normal, the deviation degree was low. For a standard normal distribution, $(-3\sigma, +3\sigma)$ contains 99.73% of all possible data. The coefficients of kurtosis of the fluctuating pressure on the steps under the different flow conditions were from 0.13 to 0.29, which indicated a narrow peak. Therefore, calculating the minimum pressure

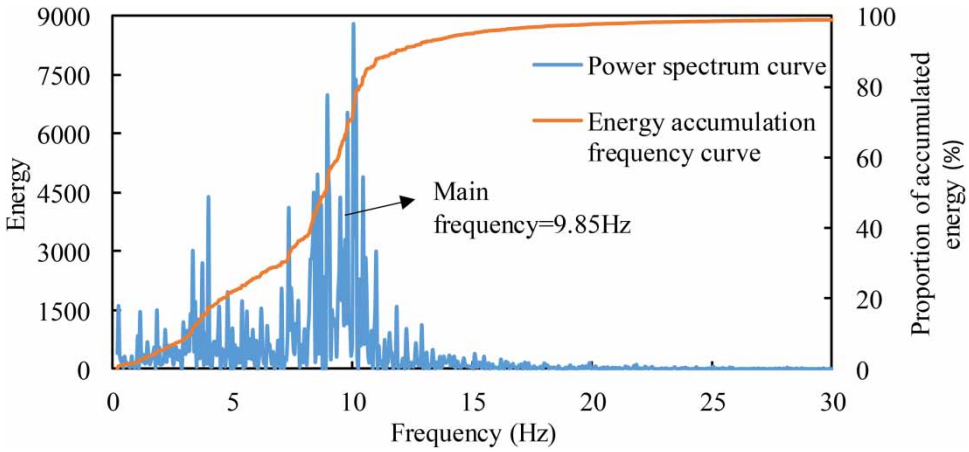

Figure 7 | Maximum pulsation main frequency in the stepped spillway under various flow conditions. The horizontal axis is the frequency, and the vertical axis is the pulsation energy and cumulative energy percentage.

as 3 times the RMS was appropriate. Therefore, the calculated minimum instantaneous pressure (p_{min}/γ) under each flow condition was −1.58 m. The calculation results of Equation (8) showed that the instantaneous water flow cavitation number in the stepped spillway was 2.61 under each flow condition. Theoretically, when $\sigma_{min} \leq 0$, cavitation would occur in the stepped spillway. Therefore, the possibility of cavitation in the stepped spillway was extremely low under the various flow conditions.

Energy dissipation

Energy dissipation in the stepped spillway dropshaft was mainly due to water cascading, crushing, strong turbulence and friction between the water flow and the step wall of the stepped spillway.

Figure 8 shows the relationship between the energy dissipation ratio (η) and the flow rate (Q^*). Under the conditions of free outflow, the energy dissipation ratio (η) decreased from 95.96% to 92.91% with an increase in the flow rate (Q^*) from 0.76 to 1.68. The energy dissipation ratio (η) increased from 68.82% to 68.95% with the increase in flow rate (Q^*) from 0.76 to 1.68 under submerged outflow conditions. In summary, the energy dissipation ratio of the stepped spillway dropshaft was higher under the strong turbulent action of the water flow in the stepped spillway.

CONCLUSIONS

This study proposed a stepped spillway dropshaft for the drainage of deep tunnels in Chengdu. Physical model tests

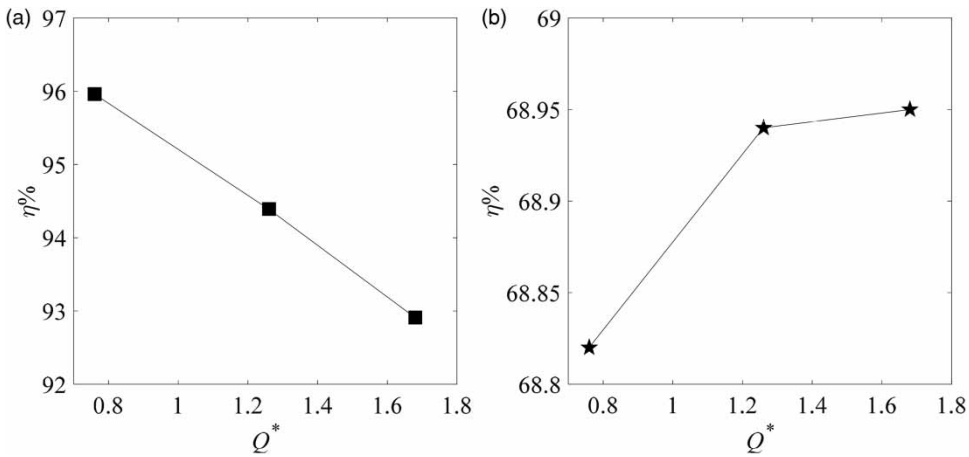

Figure 8 | Energy dissipation ratio (η) and the flow rate (Q^*).

were conducted to analyse the flow regime, aeration degree, time-averaged hydrodynamic pressure, pulsating pressure and energy dissipation ratio of the stepped spillway dropshaft. The main conclusions were as follows.

The flow regime of the stepped spillway under different flow conditions was divided into nappe flow and strong turbulent deflected jet flow. When the flow rate (Q^*) reached 1.68, the water flow on the stepped spillway exhibited a notable strike top phenomenon, which posed a safety hazard. The aeration in the stepped spillway was good under the different flow conditions. When submerged outflow occurred, the aeration in the stepped spillway was exhausted in the dropshaft through the air holes below the steps, and only a small amount of air entered the downstream tunnel, which prevented adverse phenomena, such as gas explosions, in the outlet tunnel.

According to the trend of the time-averaged hydrodynamic pressure on each step during free outflow, the pressure distribution on the step was divided into three regions, namely the recirculating region, the wall-impinging region and the mixing region. With the increase in the flow rate (Q^*), the time-averaged hydrodynamic pressure of the flow on the steps also increased. When free outflow occurred under all working conditions, the time-averaged hydrodynamic pressure on the outer side of the step was higher than the inner pressure of the step. When submerged outflow occurred, the time-averaged hydrodynamic pressure inside and outside the step did not change much.

Compared with the fluctuating strength, the maximum values of each step basically occurred at the P4 measuring point and the minimum values of each step were observed in the concave and convex areas of the step. With the increase in flow rate (Q^*), the fluctuating strength of the water flow in the stepped spillway also increased. Under different flow conditions, the pulsating pressure energy of the step measurement points was mainly concentrated within 15 Hz and the maximum main frequency was 9.85 Hz, which basically did not cause resonance of the stepped spillway. The anti-cavitation performance of the shaft was analysed from the perspective of the pulsating pressure. The results showed that the minimum water flow cavitation number was 2.61 and the possibility of cavitation was low.

The energy dissipation ratio of the stepped spillway dropshaft was high under the strong turbulent action of the water flow in the stepped spillway. The energy dissipation ratio decreased with increasing flow rate (Q^*) when free outflow occurred. The energy dissipation ratio increased with increases in the flow rate (Q^*) under various conditions of submerged outflow.

ACKNOWLEDGEMENTS

This research was funded by the National Key Project for Research and Development Plan of China (2016YFC0502207).

REFERENCES

Board, T. 2009 *Urban Stormwater Management in the United States*. Committee on Reducing Stormwater Discharge, Contributions to Water Pollution, National Research Council, The National Academies Press, New York.

Camino, G. A., Rajaratnam, N. & Zhu, D. Z. 2014 Choking conditions inside plunging flow dropshafts. *Canadian Journal of Civil Engineering* **41** (7), 624–632.

Chen, L. Q. 2014 *Research on the Energy Dissipation Mechanism and Hydraulic Characteristics of Stepped Structure in Hydraulic Tunnel[D]*. Wuhan University.

Chen, W. Z. & Gao, R. H. 2014 Review of flood disasters in Chengdu City of Sichuan Province in the past 30 years and discussion on prevention measures. *China Flood & Drought Management* **46** (3), 52–55.

Fratini, C. F., Geldof, G. D., Kluck, J. & Mikkelsen, P. S. 2012 Three points approach (3pa) for urban flood risk management: a tool to support climate change adaptation through transdisciplinarity and multifunctionality. *Urban Water Journal* **9** (5), 317–331.

Granata, F. 2016 Dropshaft cascades in urban drainage systems. *Water Science & Technology* **73** (9), 2052–2059.

Hu, L., Dai, X. H. & Tang, J. G. 2018 Analysis of key technical problems of deep drainage tunnel system. *China Water and Wastewater* **34** (8), 17–21.

Jain, S. C. 1988 Air transport in vortex-flow drop shafts. *Journal of Hydraulic Engineering* **114** (12), 1485–1497.

Jain, S. C. & Kennedy, J. F. 1983 *Vortex-flow Drop Structures for the Milwaukee Metropolitan Sewerage District Inline Storage System*. IIHR Rep. 264. Univ. of Iowa, Iowa City, IA.

Kennedy, J. F., Jain, S. C. & Quinones, R. R. 1988 Helicoidal-ramp dropshaft. *Journal of Hydraulic Engineering* **114** (3), 315–325.

Liang, C., Li, D. Q., Yuan, Z. J., Liao, Y. S., Nie, X. D., Huang, B., Wu, X. L. & Xie, Z. Y. 2019 Assessing urban flood and drought risks under climate change, China. *Hydrological Processes* **33** (9), 1349–1361.

Liu, J. H., Xia, L., Wang, H., Shao, W. W. & Ding, X. Y. 2017 Typical case analysis of deep tunnel drainage system in urban area (in Chinese). *Chinese Science Bulletin* **62** (27), 3269–3276.

Odgaard, A. J., Lyons, T. C. & Craig, A. J. 2013 Baffle-drop structure design relationships. *Journal of Hydraulic Engineering* **139** (9), 995–1002.

Qi, Y. F., Wang, Y. R. & Zhang, J. M. 2018 Three-dimensional turbulence numerical simulation of flow in a stepped dropshaft. *Water* **11** (1), 30–47.

Shen, J. Y., Wu, J. H. & Ma, F. 2019 Hydraulic characteristics of stepped spillway dropshafts. *Science China Technological Sciences* **62** (5), 868–874.

Wang, G. H., Chen, Y., Zhou, J. H., Chen, Y. L., Li, W. T., Yang, X. H. & Li, J. T. 2016 Discussion on application and development trend of deep tunnel drainage technology. *China Water and Wastewater* **32** (22), 1–6.

Wu, J. H., Yang, T., Sheng, J. Y., Ren, W. C. & Ma, F. 2018 Hydraulic characteristics of stepped spillway dropshafts with large angle. *Chinese Journal of Hydrodynamics* **33** (2), 176–180.

Yu, T., Tian, Z., Wang, W. & Xu, W. L. 2010 Investigation of fluctuating pressure for plug dissipaters. *Journal of Sichuan University (Engineering Science Edition)* **42** (3), 14–18.

Zhang, J. Y., Song, X. M., He, R. M. & Wang, X. J. 2014 Development and challenges of urban hydrology in a changing environment-I: hydrological response to urbanization. *Advances in Water Science* **25** (4), 594–605.

Zhang, J. Y., Wang, Y. T., He, R. M., Hu, Q. F. & Song, X. M. 2016 Discussion on the urban flood and waterlogging and causes analysis in China. *Advances in Water Science* **27** (4), 485–491.

Zhao, L. W., Zhu, G. & Ding, G. Q. 2016 Study of design rainstorm pattern based on construction of Sponge City in Central Area of Chengdu. *Urban Roads Bridges & Flood Control* **8** (42), 140–143.

Zhou, X. Y., Bai, Z. J. & Yang, Y. H. 2017 Linking trends in urban extreme rainfall to urban flooding in China. *International Journal of Climatology* **37** (13), 4586–4593.

First received 10 July 2019; accepted in revised form 25 November 2019. Available online 5 December 2019